

# Rigid Body Localization via Gaussian Belief Propagation with Quadratic Angle Approximation

Niclas Führling<sup>1</sup><sup>✉</sup>, Graduate Student Member, IEEE, Hyeon Seok Rou<sup>1</sup><sup>✉</sup>, Member, IEEE, Giuseppe Abreu<sup>1</sup><sup>✉</sup>, Senior Member, IEEE, David González G.<sup>2</sup><sup>✉</sup>, Senior Member, IEEE, and Osvaldo Gonsa<sup>2</sup><sup>✉</sup>

<sup>1</sup>School of Computer Science and Engineering, Constructor University, Bremen, Germany

<sup>2</sup>Wireless Communications Technologies Group, Continental AG, Frankfurt, Germany

Corresponding author: Niclas Führling (email: nfuehrling@constructor.university).

**ABSTRACT** Gaussian belief propagation (GaBP) is a technique that relies on linearized error and input-output models to yield low-complexity solutions to complex estimation problems, which has been recently shown to be effective in the design of range-based GaBP schemes for stationary and moving rigid body localization (RBL) in three-dimensional (3D) space, as long as an accurate prior on the orientation of the target rigid body is available. In this article we present a novel range-based RBL scheme via GaBP that removes the latter limitation. To this end, the proposed method incorporates a quadratic angle approximation to linearize the relative orientation between the prior and the target rigid body, enabling high precision estimates of corresponding rotation angles even for large deviations. Leveraging the resulting linearized model, we derive the corresponding message-passing (MP) rules to obtain estimates of the translation vector and rotation matrix of the target rigid body, relative to a prior reference frame. Numerical results corroborate the good performance of the proposed angle approximation itself, as well as the consequent RBL performance in terms of root mean square errors (RMSEs) in comparison to the state-of-the-art (SotA), while maintaining a low computational complexity.

**INDEX TERMS** Rigid Body Localization, Gaussian belief propagation (GaBP), Small Angle Approximation.

## I. Introduction

**S**ENSING [1] can be seen as one of the main applications in beyond fifth-generation (B5G) systems, as defined in the IMT-2030 [2] goals. In particular, the emerging integrated sensing and communications (ISAC) paradigm of new wireless standards such as sixth-generation (6G) and 802.11.bf wireless local area networks (WLANS), demonstrate that wireless systems can use radio signals not only for communications, but also to perform sensing [3], [4]. A key sensing application is to localize and detect the shape and orientation of objects of interest in the environment, which can be performed via radio-based techniques [5]. Part of the larger sensing task is wireless localization (WL) [6]–[8], whereby different properties of the radio signal such as finger-prints [9], received signal strength indicator (RSSI) [10], angle of arrival (AoA) [11], delay [12] or combinations of those [13], to estimate the location of targets. But more sophisticated sensing-driven applications such as autonomous driving and

robotic systems require capabilities including navigation [14], collision detection [15], and vehicle trajectory and path prediction [16], which in turn demand not only accurate position estimates of point targets, but more detailed and reliable information about the shape and orientation of three-dimensional (3D) objects [17], [18].

This requirement gives rise to a localization paradigm known as rigid body localization (RBL) [19]–[28]. To elaborate, while traditional WL schemes are designed to estimate the positions of individual point-targets independently, the objective of RBL technology is to jointly estimate the global translation and attitude (jointly referred to as pose) of a 3D object, based on a collection of landmark points whose positions are fixed relative to one another due to the rigid shape of the object.

Existing approaches for estimating the location and attitude of rigid objects span multiple sensing modalities. For instance, computer vision-based methods typically rely on

pose estimation from image or video data [29], [30]. While effective in controlled environments, these approaches often require large data volumes and computationally intensive processing, which can limit their applicability in resource-constrained or real-time systems. Alternatively, inertial measurement unit (IMU)-based techniques exploit measurements from accelerometers, gyroscopes, and magnetometers to infer orientation and motion [31], [32]. However, such methods are prone to drift, require frequent recalibration, and often depend on external aiding technologies, thereby partially undermining their self-contained nature.

In contrast to the aforementioned approaches, the wireless RBL framework considered in this work [19], [20], [22], [25]–[27] extends the conventional range-based WL paradigm to the RBL problem, by explicitly exploiting range measurements between landmark points<sup>1</sup> on the rigid body and a set of *anchor* nodes at known positions [33], [34]. This formulation enables the joint estimation of the rigid body's global position, orientation, and, when applicable, its geometric configuration. Earlier state-of-the-art (SotA) contributions to range-based RBL approaches are based on either algebraic methods leveraging multidimensional scaling (MDS) [28], super multidimensional scaling (SMDS) [35] or semi-definite relaxation (SDR) [36], [37], all of which have a cubic computational complexity at least.

A representative example of a well-balanced solution that combines high estimation accuracy with moderate computational complexity is the least squares (LS) method proposed in [22]. In the scheme thereby, preliminary position estimates for the individual landmark points are first obtained from range measurements via a LS formulation based on the linearized model in [38]. The rigid body translation and rotation are then extracted using a singular value decomposition (SVD)-based procedure, followed by a refinement step that enforces the rigid body constraints through an Euler-angle parametrization solved via weighted least square (WLS).

The ability of the method in [22] to solve the RBL problem within a unified framework stems from the use of linearized error models on the measured square distances [38], [39]. Nevertheless, the reliance on LS formulations and multi-stage processing can limit estimation performance, particularly in scenarios with strongly coupled variables [40], as well as the fact that a small angle approximation is used in the linearized model. In terms of complexity, message-passing-based methods [41] are well known to offer favorable accuracy-complexity trade-offs in such settings. These methods enable efficient inference either through alternating schemes [42] or through joint bilinear formulations [5], [43]–[45]. There are multiple message passing-based localization techniques in the WL literature, though not specifically designed for RBL, for example, the method presented in [46], where a RSSI-based cooperative localization prob-

lem involving an unknown path loss exponent is solved via message passing algorithms that solve a probabilistic inference problem. In terms of sensing applications, [47] employs Gaussian belief propagation (GaBP) for simultaneous localization and synchronization based on time of arrival (ToA) measurements, while [48] leverages GaBP for distributed multiple-input multiple-output (MIMO) radar localization, resulting in low computational complexity and reduced communication cost.

The most recent, and to the best of the authors' knowledge, the only message passing-based method specifically designed for RBL methods are presented in [49], [50], where the linearized model in [22] is leveraged in the design of multiple linear and bilinear GaBP algorithms for estimation of rigid body parameters both in stationary and moving scenarios, that is, yielding estimates for both the translation and rotation, as well as the angular and translational velocities of the rigid body. However, a limitation of the linearized system model used in [22] and [50], as mentioned above, is that it relies on the small angle approximation of the rotation matrix, which is only valid for very small angles, typically below 10° [51] and significantly degrades the performance for larger angle deviations, as shown in [50].

In view of the above, based on our work in [49], we propose in this article a GaBP-based approach for RBL, in which we use a novel quadratic approximation of the rotation matrix, instead of the commonly used small angle approximation, which is only valid for very small angles. To that extent, we derive a linearized system model that uses the proposed quadratic angle approximation of the rotation matrix, which is then used in a modified bilinear GaBP algorithm to estimate the rigid body parameters, *i.e.*, the translation and rotation of the target rigid body.

Our contributions can be summarized as follows:

- A novel vectorized model of the 3D rotation matrix via a quadratic angle approximation is proposed, which is valid for large angle deviations between the orientations of the prior and true target.
- A new linearized system model for RBL is derived based on the proposed quadratic angle approximation that relates the range measurements directly to the rigid body parameters and enables the use of GaBP-based estimation.
- A new bilinear GaBP algorithm is presented to estimate the rigid body parameters, *i.e.*, translation and rotation, based on the proposed linearized system model.

The structure of the remainder of the article is as follows. First, the rigid body system model, as well as the measurement model is described in Section II. Next, in Section III, the proposed linearized system model via the quadratic angle approximation is introduced, followed by the modified GaBP algorithm used to estimate the rigid body parameters. Finally, a comparison of the proposed scheme with the small angle approximation, GaBP-based RBL method is presented in Section IV.

<sup>1</sup>Landmark points can either represent edges and corners passively detected via radar-like methods, or actual sensors located at the rigid body. In this article we focus on RBL algorithms rather than ranging methods, and such that both approaches can be abstracted as equivalent.

## II. Rigid Body Localization System Model

### A. Rigid Body System Model

Consider, as illustrated in Figure 1, a scenario where a rigid body consisting of  $N$  landmark points is transformed – that is changes its pose – in 3D Euclidean space. Each sensor of the rigid body is described by a  $3 \times 1$  vector denoted by  $\mathbf{c}_n \in \mathbb{R}^{3 \times 1}$  for  $n = \{1, \dots, N\}$ . The conformation matrix, describing the initial reference position of the rigid body is therefore defined by  $\mathbf{C} = [\mathbf{c}_1, \mathbf{c}_2, \dots, \mathbf{c}_N] \in \mathbb{R}^{3 \times N}$  at the reference frame (local axis) of the rigid body.

To define the transformation of the rigid body in 3D space, a translation and rotation needs to be introduced, respectively described by the translation vector  $\mathbf{t} \triangleq [t_x, t_y, t_z]^\top \in \mathbb{R}^{3 \times 1}$  consisting of the translation distances for each axis, and a 3D rotation matrix<sup>2</sup>  $\mathbf{Q} \in \mathbb{R}^{3 \times 3}$  given by equation (1), where  $\mathbf{Q}_x, \mathbf{Q}_y, \mathbf{Q}_z \in \mathbb{R}^{3 \times 3}$  are the roll, pitch, and yaw rotation matrices about the  $x$ -,  $y$ -,  $z$ -axes by rotation angles of  $\theta_x, \theta_y, \theta_z \in [-180^\circ, 180^\circ]$  degrees, respectively.

Next, the transformed coordinates of the  $n$ -th sensor after the rotation and translation is described by

$$\mathbf{s}_n = \mathbf{Q}\mathbf{c}_n + \mathbf{t} \in \mathbb{R}^{3 \times 1}, \quad (2)$$

which is applied identically to all  $N$  landmark points of the rigid body, as illustrated in Figure 1, such that for the full body, the equation can be rewritten as

$$\mathbf{S} = \mathbf{Q}\mathbf{C} + \mathbf{t}\mathbf{1}_N^\top \in \mathbb{R}^{3 \times 1}, \quad (3)$$

where  $\mathbf{1}_N$  denotes a column vector of length  $N$ .

Finally, as illustrate in Figure 2, in order to perform measurements for the localization, the target rigid body is surrounded by a total of  $M$  reference sensors (hereafter referred simply as anchors), defined by their known location  $\mathbf{a}_m \in \mathbb{R}^{3 \times 1}$  for  $m = \{1, \dots, M\}$ .

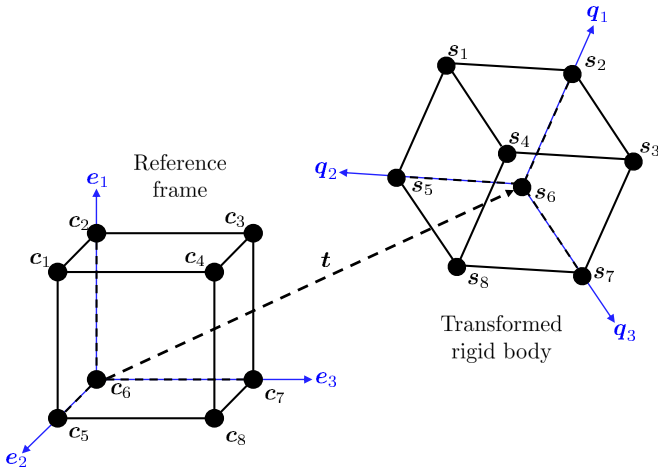


**Figure 1.** An illustration of the transformation of a rigid body, whose location has a 3D rotation  $\mathbf{Q}$  and a translation  $\mathbf{t}$  applied to the reference frame, as determined by equation (2).

<sup>2</sup>The rotation matrix  $\mathbf{Q}$  is part of the special orthogonal group such that  $SO(3) = \{\mathbf{Q} \in \mathbb{R}^{3 \times 3} : \mathbf{Q}^\top \mathbf{Q} = \mathbf{I}, \det(\mathbf{Q}) = 1\}$  [51] needs to hold.

### B. Measurement Model

The pairwise range measurements between anchors and landmark points considered for RBL, assumed to be available by a common processing unit, are described by

$$\tilde{d}_{m,n} = d_{m,n} + w_{m,n} = \|\mathbf{a}_m - \mathbf{s}_n\|_2 + w_{m,n} \in \mathbb{R}, \quad (4)$$

where corresponding conventional squared range measurements are modeled as

$$\tilde{d}_{m,n}^2 = \|\mathbf{a}_m - \mathbf{s}_n\|_2^2 + 2d_{m,n}w_{m,n} + w_{m,n}^2 \in \mathbb{R}, \quad (5)$$

with  $w_{m,n} \sim \mathcal{N}(0, \sigma_w^2)$  denoting the independent and identically distributed (i.i.d.) additive white Gaussian noise (AWGN) of variance  $\sigma_w^2$  affecting the range measurement, while  $d_{m,n} \triangleq \|\mathbf{a}_m - \mathbf{s}_n\|_2$  is the true Euclidean distance between the  $m$ -th anchor and the  $n$ -th sensor.

Following [22], [52], [53], the range measurement equation in (5) can be reformulated in terms of a linear relation with a *composite ranging noise*  $\xi_n \in \mathbb{R}$  defined as

$$\xi_{m,n} = \tilde{d}_{m,n}^2 - \|\mathbf{a}_m\|_2^2 - \|\mathbf{s}_n\|_2^2 + 2\mathbf{a}_m^\top \mathbf{s}_n \approx 2d_{m,n}w_{m,n}, \quad (6)$$

where the second-order noise term  $w_{m,n}^2$  is neglected.

By rearranging and stacking equation (6) for all  $M$  anchors, the system can be reformulated as a linear system on the  $n$ -th unknown sensor variable, which yields

$$\mathbf{y}_n \triangleq \begin{bmatrix} \tilde{d}_{1,n}^2 - \|\mathbf{a}_1\|_2^2 \\ \vdots \\ \tilde{d}_{M,n}^2 - \|\mathbf{a}_M\|_2^2 \end{bmatrix} = \begin{bmatrix} -2\mathbf{a}_1^\top, 1 \\ \vdots \\ -2\mathbf{a}_M^\top, 1 \end{bmatrix} \underbrace{\begin{bmatrix} \mathbf{s}_n \\ \|\mathbf{s}_n\|_2^2 \end{bmatrix}}_{\triangleq \mathbf{x}_n \in \mathbb{R}^{4 \times 1}} + \underbrace{\begin{bmatrix} \xi_{1,n} \\ \vdots \\ \xi_{M,n} \end{bmatrix}}_{\triangleq \xi_n \in \mathbb{R}^{M \times 1}}, \quad (7)$$

where,  $\mathbf{y}_n \in \mathbb{R}^{M \times 1}$  denotes the observed data vector,  $\mathbf{G} \in \mathbb{R}^{M \times 4}$  denotes the effective channel matrix, which has been implicitly defined to be constructed from range measurements and anchor positions  $\mathbf{a}_m$ .

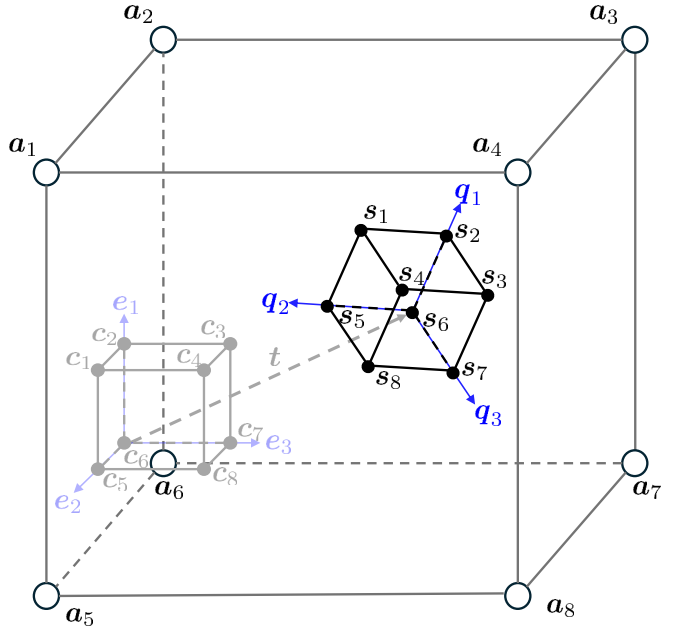


**Figure 2.** Illustration of the transformed rigid body surrounded by  $M$  anchors, whose locations are known.

$$\begin{aligned}
\mathbf{Q} &\triangleq \mathbf{Q}_z(\theta_z) \mathbf{Q}_y(\theta_y) \mathbf{Q}_x(\theta_x) = \underbrace{\begin{bmatrix} \cos \theta_z & -\sin \theta_z & 0 \\ \sin \theta_z & \cos \theta_z & 0 \\ 0 & 0 & 1 \end{bmatrix}}_{\triangleq \mathbf{Q}_z \in \mathbb{R}^{3 \times 3}} \cdot \underbrace{\begin{bmatrix} \cos \theta_y & 0 & \sin \theta_y \\ 0 & 1 & 0 \\ -\sin \theta_y & 0 & \cos \theta_y \end{bmatrix}}_{\triangleq \mathbf{Q}_y \in \mathbb{R}^{3 \times 3}} \cdot \underbrace{\begin{bmatrix} 1 & 0 & 0 \\ 0 & \cos \theta_x & -\sin \theta_x \\ 0 & \sin \theta_x & \cos \theta_x \end{bmatrix}}_{\triangleq \mathbf{Q}_x \in \mathbb{R}^{3 \times 3}} \quad (1) \\
&= \begin{bmatrix} \cos \theta_y \cos \theta_z & \sin \theta_x \sin \theta_y \cos \theta_z - \cos \theta_x \sin \theta_z & \cos \theta_x \sin \theta_y \cos \theta_z + \sin \theta_x \sin \theta_z \\ \cos \theta_y \sin \theta_z & \sin \theta_x \sin \theta_y \sin \theta_z + \cos \theta_x \cos \theta_z & \cos \theta_x \sin \theta_y \sin \theta_z - \sin \theta_x \cos \theta_z \\ -\sin \theta_y & \sin \theta_x \cos \theta_y & \cos \theta_x \cos \theta_y \end{bmatrix} = \begin{bmatrix} q_{1,1} & q_{1,2} & q_{1,3} \\ q_{2,1} & q_{2,2} & q_{2,3} \\ q_{3,1} & q_{3,2} & q_{3,3} \end{bmatrix}.
\end{aligned}$$

In the above, the vector  $\mathbf{x}_n \in \mathbb{R}^{4 \times 1}$  is implicitly defined, which contains the unknown coordinates of the  $n$ -sensor, as well as its distance to the origin, while the vector  $\xi_n \in \mathbb{R}^{M \times 1}$  gathers the composite noise quantities defined in equation (6).

As shown in [50], the linear system in equation (7) can be leveraged for the estimation of the unknown sensor coordinate vector  $\mathbf{s}_n$  and sensor position norm  $\|\mathbf{s}\|_2^2$  in  $\mathbf{x}_n$  via a linear GaBP approach. With the estimate of the sensor positions in hand, equation (2) can either be invoked for the translation and rotation extraction via Procrustes analysis or other classical algorithms [54], as described in [22], or a bivariate GaBP approach can be invoked to estimate the rigid body parameters directly, as described in [49], where a small angle approximation was used to linearize the rotation matrix to enable the GaBP approach.

### C. SotA Parameter-based System Model via Small Angle Approximation

As proposed in [50], equation (7) can be reformulated, such that system variables can be expressed directly in terms of the RBL transformation parameters, *i.e.*, the 3D rotation angles  $\boldsymbol{\theta} \triangleq [\theta_x, \theta_y, \theta_z]^\top \in \mathbb{R}^{3 \times 1}$  and translation vector  $\mathbf{t}$  [55]. To enable the reformulation, first, a small-angle approximation<sup>3</sup> [51] is applied onto the rotation matrix of equation (1), obtained by the approximations  $\cos \theta \approx 1$  and  $\sin \theta \approx \theta$ , which yields

$$\mathbf{Q} \approx \begin{bmatrix} 1 & \theta_z & -\theta_y \\ -\theta_z & 1 & \theta_x \\ \theta_y & -\theta_x & 1 \end{bmatrix} \in \mathbb{R}^{3 \times 3}, \quad (8)$$

which can be vectorized into a linear system directly in terms of the Euler angles  $\boldsymbol{\theta}$  [22], given by

$$\begin{aligned}
\text{vec}(\mathbf{Q}) &= \underbrace{\boldsymbol{\gamma} + \mathbf{L}\boldsymbol{\theta}}_{\triangleq \boldsymbol{\gamma} \in \mathbb{R}^{9 \times 1}} = \underbrace{\begin{bmatrix} 1 & 0 & 0 & 0 & 1 & 0 & 0 & 0 & 1 \end{bmatrix}^\top}_{\triangleq \mathbf{L} \in \mathbb{R}^{9 \times 3}} \\
&+ \underbrace{\begin{bmatrix} 0 & 1 & 0 & -1 & 0 & 0 & 0 & 0 & 0 \end{bmatrix}^\top}_{\triangleq \mathbf{L} \in \mathbb{R}^{9 \times 3}} \cdot \begin{bmatrix} \theta_x \\ \theta_y \\ \theta_z \end{bmatrix}. \quad (9)
\end{aligned}$$

<sup>3</sup>For practical rigid body tracking applications, subsequent transformation estimations can be assumed to be performed within a sufficiently short time interval such that the change in rotation angle remains small. Although the approximation remains valid for rotation angles up to approximately twenty degrees, convergence of the algorithm can still be achieved for larger angles. However, in such cases, the estimation accuracy may degrade.

Next, when equation (9) is substituted into equations (2) and (6) and the terms are rearranged, an alternate representation of the composite noise is obtained, given by

$$\begin{aligned}
\xi_n &= \tilde{d}_{m,n}^2 - \|\mathbf{a}_m\|_2^2 - \|\mathbf{s}_n\|_2^2 + 2[\mathbf{c}_n^\top \otimes \mathbf{a}_m^\top] \boldsymbol{\gamma} \\
&\quad + 2[\mathbf{c}_n^\top \otimes \mathbf{a}_m^\top] \mathbf{L} \boldsymbol{\theta} + 2\mathbf{a}_m^\top \mathbf{t} \in \mathbb{R},
\end{aligned} \quad (10)$$

where  $\otimes$  denotes the Kronecker product operator and vectorization identity of the matrix product  $\text{vec}(\mathbf{XYZ}) = (\mathbf{Z}^\top \otimes \mathbf{X}) \text{vec}(\mathbf{Y})$  has been used.

Finally, the fundamental system can be rewritten as a linearization of equation (10) in terms of the rigid body parameters  $\boldsymbol{\theta}$  and  $\mathbf{t}$ , which yields

$$\mathbf{z}_n = \mathbf{H}_\theta \cdot \boldsymbol{\theta} + \mathbf{H}_t \cdot \mathbf{t} + \xi_n \in \mathbb{R}^{M \times 1}, \quad (11a)$$

with

$$\mathbf{z}_n = \begin{bmatrix} \tilde{d}_{1,n}^2 - \|\mathbf{a}_1\|_2^2 - \|\mathbf{s}_n\|_2^2 + 2[\mathbf{c}_n^\top \otimes \mathbf{a}_1^\top] \boldsymbol{\gamma} \\ \vdots \\ \tilde{d}_{M,n}^2 - \|\mathbf{a}_M\|_2^2 - \|\mathbf{s}_n\|_2^2 + 2[\mathbf{c}_n^\top \otimes \mathbf{a}_M^\top] \boldsymbol{\gamma} \end{bmatrix} \in \mathbb{R}^{M \times 1}, \quad (11b)$$

where  $\mathbf{z}_n \in \mathbb{R}^{M \times 1}$  denotes the effective observed data vector,  $\xi_n \in \mathbb{R}^{M \times 1}$  is the vector of composite noise variables from equation (6), and  $\mathbf{H}_\theta$  and  $\mathbf{H}_t$  are the two effective channel matrices for rotation and translation respectively, given by

$$\mathbf{H}_\theta = \begin{bmatrix} -2[\mathbf{c}_i^\top \otimes \mathbf{a}_1^\top] \mathbf{L} \\ \vdots \\ -2[\mathbf{c}_i^\top \otimes \mathbf{a}_M^\top] \mathbf{L} \end{bmatrix} \in \mathbb{R}^{M \times 3}, \quad (11c)$$

and

$$\mathbf{H}_t = \begin{bmatrix} -2\mathbf{a}_1^\top \\ \vdots \\ -2\mathbf{a}_M^\top \end{bmatrix} \in \mathbb{R}^{M \times 3}. \quad (11d)$$

### III. Proposed method

In light of the above, the proposed method proposes a reformulation of the linear system proposed in [50] by the introduction of a quadratic angle approximation, which is then used in a modified GaBP algorithm to estimate the rigid body parameters directly.

#### A. System Model via Quadratic Angle Approximation

Instead of the conventional small angle approximation, where  $\sin \theta \approx \theta$  and  $\cos \theta \approx 1$ , we propose a novel quadratic approximation of the rotation matrix. To that extent, we approximate the elements of a rotation matrix  $\mathbf{Q}^{[i]} \in \mathbb{R}^{3 \times 3}$  using a quadratic approximation, based on

$$\sin(\theta) \approx \alpha \theta^{[i-1]} \theta^{[i]} + \beta \theta^{[i]}, \quad (12a)$$

$$\cos(\theta) \approx \gamma - \delta \theta^{[i-1]} \theta^{[i]}, \quad (12b)$$

where the values for the parameters  $\alpha, \beta, \gamma, \delta \in \mathbb{R}$  are chosen such that the approximation is as accurate as possible in the interval  $\theta \in [-\pi/4, \pi/4]$ . To that extent, for the sine approximation, we use  $\alpha^+$  for positive angles and  $\alpha^-$  for negative angles, while for the cosine approximation the same parameters are used for positive and negative angles. In order to ensure that the approximations pass through the origin and the exact value at  $\pi/4$ , as shown in Figure 3, the parameters are chosen as described in Table 1. Finally, in order to linearize the model to be applicable in the proposed GaBP, however,  $\theta^{[i-1]}$  has to be known from the previous iteration and  $\theta^{[i]}$  is the current unknown.

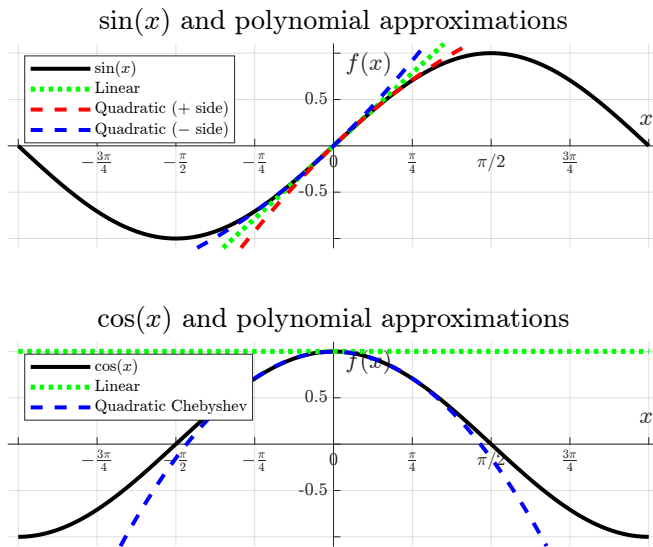


**Figure 3.** Various Sine and Cosine approximations  
 $\sin(x)$  : Absolute error  $|\hat{f} - f|$  of approximations

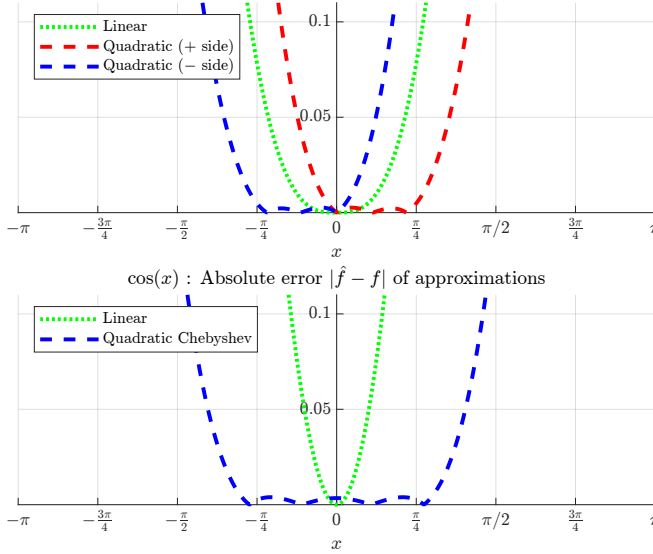


**Figure 4.** Errors of the Sine and Cosine approximations

**Table 1.** Parameters used for the sine and cosine approximations.

| Parameter  | Value             | Used for              |
|------------|-------------------|-----------------------|
| $\alpha^+$ | -0.16884          | sine ( $\theta > 0$ ) |
| $\alpha^-$ | +0.16884          | sine ( $\theta < 0$ ) |
| $\beta$    | 1.03912           | cosine                |
| $\gamma$   | $\frac{577}{579}$ | cosine                |
| $\delta$   | $\frac{274}{589}$ | cosine                |

Following the procedure as in (9), as derived in Appendix A, we then represent the vectorized matrix as an affine-linear function of  $\theta^{[i]}$ , which yields

$$\text{vec}(\mathbf{Q}^{[i]}) = \gamma + (\beta \mathbf{L} + \alpha \mathbf{L}\Theta - \delta \mathbf{D}\Theta) \theta^{[i]}, \quad (13)$$

where  $\theta^{[i]} = [\theta_x^{[i]}, \theta_y^{[i]}, \theta_z^{[i]}]^\top \in \mathbb{R}^{3 \times 1}$  denotes the unknown current angles and  $\theta^{[i-1]} = [\theta_x^{[i-1]}, \theta_y^{[i-1]}, \theta_z^{[i-1]}]^\top \in \mathbb{R}^{3 \times 1}$  the known previous angles. The diagonal matrix  $\Theta = \text{diag}(\theta^{[i-1]}) \in \mathbb{R}^{3 \times 3}$  collects the previous angles on its diagonal. Furthermore, the constant vector is given by  $\gamma = \gamma^2 \cdot \text{vec}(\mathbf{I}_3) = \gamma^2 [1, 0, 0, 0, 1, 0, 0, 0, 1]^\top$ . The matrices  $\mathbf{L}, \mathbf{D} \in \mathbb{R}^{9 \times 3}$  are defined as

$$\mathbf{L} = \begin{bmatrix} 0 & 0 & 0 & 0 & 0 & \gamma & 0 & -\gamma & 0 \end{bmatrix}^\top, \quad (14a)$$

$$\mathbf{D} = \begin{bmatrix} 0 & 0 & 0 & 0 & 1 & 0 & 0 & 0 & 1 \end{bmatrix}^\top. \quad (14b)$$

As shown in Figure 4, the quadratic approximation yields a significantly lower error compared to the small angle approximation, especially for angles larger than  $20^\circ$ . In particular, for the cosine approximation, the maximum error for angles up to  $45^\circ$  is reduced from approximately 0.08 to less than 0.005. For the sine approximation, the maximum error is reduced from approximately 0.3 to less than 0.004. While the approximation error is still increasing for angles larger than  $45^\circ$ , the proposed approximation still yields a significantly lower error compared to the small angle approximation, which could be improved further by using higher order approximations, which is left for future work.

### B. Proposed Linear Model

In light of the above, the fundamental system in equation (11) can be rewritten leveraging the linear quadratic approximation of equation (13), which yields

$$\mathbf{z}_n = \mathbf{H}_\theta \cdot \theta + \mathbf{H}_t \cdot \mathbf{t} + \boldsymbol{\xi}_n \in \mathbb{R}^{M \times 1}, \quad (15a)$$

where  $\mathbf{z}_n \in \mathbb{R}^{M \times 1}$ ,  $\boldsymbol{\xi}_n \in \mathbb{R}^{M \times 1}$ , and  $\mathbf{H}_t$ , are identical to the previous terms, while the effective channel matrix for the rotation is redefined as

$$\mathbf{H}_\theta = \begin{bmatrix} -2[\mathbf{c}_1^\top \otimes \mathbf{a}_1^\top] (\beta \mathbf{L} + \alpha \mathbf{L}\Theta - \delta \mathbf{D}\Theta) \\ \vdots \\ -2[\mathbf{c}_M^\top \otimes \mathbf{a}_M^\top] (\beta \mathbf{L} + \alpha \mathbf{L}\Theta - \delta \mathbf{D}\Theta) \end{bmatrix} \in \mathbb{R}^{M \times 3}. \quad (15b)$$

Finally, it has to be ensured that, depending on the prior angles  $\theta^{[i-1]}$ , the correct approximation parameters is used, as shown by Figure 3, where there exists a plus and minus side for the approximation.

### C. Bivariate GaBP for Rigid Body Parameter Estimation

With the linear formulation of the system model in hand, the message passing rules for the GaBP iterations need to be defined, which are similar to the algorithm shown in [50], where in the case of transformation parameter estimation using the new model based on equation (15), there exist two sets of variables  $\theta_k$  with  $k \in \{1, \dots, K\}$  and  $t_\ell$  with  $\ell \in \{1, \dots, K\}$ , where  $K$  is the dimension of the rigid body parameters to be estimated, *i.e.*,  $K = 3$  in 3D space, such that the GaBP rules are elaborated separately, updating the model every iteration.

To perform the GaBP estimation, first soft interference cancellation (soft-IC) is performed on the observed information for rigid body parameters, *i.e.*, the rotation angles and translation as

$$\begin{aligned} \tilde{z}_{\theta:m,k}^{[j]} &= z_m - \sum_{i \neq k} h_{\theta:m,i} \hat{\theta}_{m,i}^{[j]} - \sum_{i=1}^K h_{t:m,i} \hat{t}_{m,i}^{[j]}, \quad (16a) \\ &= h_{\theta:m,k} \theta_k + \sum_{i=1}^K h_{t:m,i} (t_i - \hat{t}_{m,i}^{[j]}) \\ &\quad + \sum_{i \neq k} h_{\theta:m,i} (\theta_i - \hat{\theta}_{m,i}^{[j]}) + \xi_m, \end{aligned}$$

$$\begin{aligned} \tilde{z}_{t:m,\ell}^{[j]} &= z_m - \sum_{i=1}^K h_{\theta:m,i} \hat{\theta}_{m,i}^{[j]} - \sum_{i \neq \ell} h_{t:m,i} \hat{t}_{m,i}^{[j]}, \quad (16b) \\ &= h_{t:m,\ell} t_\ell + \sum_{i=1}^K h_{\theta:m,i} (\theta_i - \hat{\theta}_{m,i}^{[j]}) \\ &\quad + \sum_{i \neq \ell} h_{t:m,i} (t_i - \hat{t}_{m,i}^{[j]}) + \xi_m. \end{aligned}$$

Thus, the conditional probability density functions (PDFs) of the soft-IC symbols are defined as

$$p_{\tilde{z}_{\theta:m,k}^{[j]} | \theta_k} (\tilde{z}_{\theta:m,k}^{[j]} | \theta_k) \propto \exp \left[ - \frac{|\tilde{z}_{\theta:m,k}^{[j]} - h_{\theta:m,k} \theta_k|^2}{\sigma_{\theta:m,k}^{2[j]}} \right], \quad (17a)$$

$$p_{\tilde{z}_{t:m,\ell}^{[j]} | t_\ell} (\tilde{z}_{t:m,\ell}^{[j]} | t_\ell) \propto \exp \left[ - \frac{|\tilde{z}_{t:m,\ell}^{[j]} - h_{t:m,\ell} t_\ell|^2}{\sigma_{t:m,\ell}^{2[j]}} \right], \quad (17b)$$

with the corresponding conditional variances given by

$$\sigma_{\theta:m,k}^{2[j]} = \sum_{i \neq k} |h_{\theta:m,i}|^2 \psi_{\theta:m,i}^{[j]} + \sum_{i=1}^K |h_{t:m,i}|^2 \psi_{t:m,i}^{[j]} + N_0 \in \mathbb{R}, \quad (18a)$$

$$\sigma_{t:m,\ell}^{2[j]} = \sum_{i=1}^K |h_{\theta:m,i}|^2 \psi_{\theta:m,i}^{[j]} + \sum_{i \neq \ell} |h_{t:m,i}|^2 \psi_{t:m,i}^{[j]} + N_0 \in \mathbb{R}, \quad (18b)$$

where the corresponding mean square errors (MSEs) are defined as

$$\psi_{\theta:m,k}^{[j]} = \mathbb{E}_{\theta_k} [|\theta_k - \hat{\theta}_{m,k}^{[j]}|^2], \quad (18c)$$

$$\psi_{t:m,\ell}^{[j]} = \mathbb{E}_{t_\ell} [|t_\ell - \hat{t}_{m,\ell}^{[j]}|^2]. \quad (18d)$$

Since the conditional PDF is known, the extrinsic PDF can be found next via

$$\prod_{i \neq m} p_{\tilde{z}_{\theta:i,k}^{[j]} | \theta_k} (\tilde{z}_{\theta:i,k}^{[j]} | \theta_k) \propto \exp \left[ - \frac{|\theta_k - \hat{\theta}_{m,k}^{[j]}|^2}{\bar{v}_{\theta:m,k}^{[j]}} \right], \quad (19)$$

$$\prod_{i \neq m} p_{\tilde{z}_{t:i,\ell}^{[j]} | t_\ell} (\tilde{z}_{t:i,\ell}^{[j]} | t_\ell) \propto \exp \left[ - \frac{|t_\ell - \hat{t}_{m,\ell}^{[j]}|^2}{\bar{v}_{t:m,\ell}^{[j]}} \right],$$

with the extrinsic means and variances are defined as

$$\bar{\theta}_{m,k}^{[j]} = \bar{v}_{\theta:m,k}^{[j]} \left( \sum_{i \neq m} \frac{h_{\theta:i,k} \cdot \tilde{z}_{\theta:i,k}^{[j]}}{(\sigma_{\theta:i,k}^{[j]})^2} \right) \in \mathbb{R}, \quad (20a)$$

$$\bar{t}_{m,\ell}^{[j]} = \bar{v}_{t:m,\ell}^{[j]} \left( \sum_{i \neq m} \frac{h_{t:i,\ell} \cdot \tilde{z}_{t:i,\ell}^{[j]}}{(\sigma_{t:i,\ell}^{[j]})^2} \right) \in \mathbb{R}, \quad (20b)$$

$$\bar{v}_{\theta:m,k}^{[j]} = \left( \sum_{i \neq m} \frac{|h_{\theta:i,k}|^2}{(\sigma_{\theta:i,k}^{[j]})^2} \right)^{-1} \in \mathbb{R}, \quad (21a)$$

$$\bar{v}_{t:m,\ell}^{[j]} = \left( \sum_{i \neq m} \frac{|h_{t:i,\ell}|^2}{(\sigma_{t:i,\ell}^{[j]})^2} \right)^{-1} \in \mathbb{R}. \quad (21b)$$

Finally, the denoisers with a Gaussian prior are given by

$$\check{\theta}_{m,k} = \frac{\phi_\theta \cdot \bar{\theta}_{m,k}^{[j]}}{\phi_\theta + \bar{v}_{\theta:m,k}^{[j]}} \in \mathbb{R}, \quad \check{t}_{m,\ell} = \frac{\phi_t \cdot \bar{t}_{m,\ell}^{[j]}}{\phi_t + \bar{v}_{t:m,\ell}^{[j]}} \in \mathbb{R}, \quad (22a)$$

$$\check{\psi}_{\theta:m,k} = \frac{\phi_\theta \cdot \bar{v}_{\theta:m,k}^{[j]}}{\phi_\theta + \bar{v}_{\theta:m,k}^{[j]}} \in \mathbb{R}, \quad \check{\psi}_{t:m,\ell} = \frac{\phi_t \cdot \bar{v}_{t:m,\ell}^{[j]}}{\phi_t + \bar{v}_{t:m,\ell}^{[j]}} \in \mathbb{R}, \quad (22b)$$

where  $\phi_\theta$  and  $\phi_t$  are the variance of the individual elements in  $\theta$  and  $t$ .

Subsequently, the soft-replicas are iteratively updated via

$$\hat{x}_{m,k}^{[j+1]} = \rho \hat{x}_{m,k}^{[j]} + (1 - \rho) \check{x}_{m,k}^{[j]}, \quad (23a)$$

$$\hat{\psi}_{m,k}^{[j+1]} = \rho \hat{\psi}_{m,k}^{[j]} + (1 - \rho) \check{\psi}_{m,k}^{[j]}, \quad (23b)$$

where  $\rho$  is the damping factor, while the algorithm performs  $j_{\max}$  iterations of the message passing method or until a convergence criteria is met, after which the consensus estimates are obtained as

$$\tilde{\theta}_k = \left( \sum_{m=1}^M \frac{|h_{\theta:m,k}|^2}{(\sigma_{\theta:m,k}^{[j_{\max}]})^2} \right)^{-1} \left( \sum_{m=1}^M \frac{h_{\theta:m,k} \cdot \tilde{z}_{\theta:m,k}^{[j_{\max}]}}{(\sigma_{\theta:m,k}^{[j_{\max}]})^2} \right) \in \mathbb{R}, \quad (24a)$$

$$\tilde{t}_\ell = \left( \sum_{m=1}^M \frac{|h_{t:m,\ell}|^2}{(\sigma_{t:m,\ell}^{[j_{\max}]})^2} \right)^{-1} \left( \sum_{m=1}^M \frac{h_{t:m,\ell} \cdot \tilde{z}_{t:m,\ell}^{[j_{\max}]}}{(\sigma_{t:m,\ell}^{[j_{\max}]})^2} \right) \in \mathbb{R}. \quad (24b)$$

Even though the message passing rules described by equations (16)-(24) are complete to yield the estimated rotation angles and translation vectors, there is a difference in effective channel powers of  $\mathbf{H}_\theta$  and  $\mathbf{H}_t$  in equation (11), where the latter is typically much larger, resulting from the absolute positions of the anchors and landmark points, which lead to good estimates of the translation vector elements, but poor estimates of the rotation angles in a joint estimation described by the GaBP procedure.

**Algorithm 1** : Double GaBP for RBL Parameter Estimation

**Input:**  $\mathbf{z}_n$  ( $\|\mathbf{s}_n\|_2^2$ )  $\forall n$ ,  $\mathbf{H}_\theta$ ,  $\mathbf{H}_t$ ,  $\phi_\theta$ ,  $\phi_t$ ,  $N_0$ ,  $j_{\max}$ ,  $\rho$ .

**Output:**  $\tilde{\theta}_k$  and  $\tilde{t}_\ell$   $\forall k, \ell$  (for all sensor nodes  $\forall n$ );

 Perform  $\forall n, m, k, \ell$  :

- 1: Initialize  $\hat{\theta}_{m,k}^{[1]}$ ,  $\hat{t}_{m,\ell}^{[1]}$ ,  $\psi_{\theta:m,k}^{[1]}$ ,  $\psi_{t:m,\ell}^{[1]}$ ;
- 2: **for**  $j = 1$  to  $j_{\max}$  **do**
- 3: Compute soft-IC symbols  $\tilde{z}_{\theta:m,k}^{[j]}$ ,  $\tilde{z}_{t:m,\ell}^{[j]}$  via eq. (16);
- 4: Compute conditional variances  $\sigma_{\theta:m,k}^{2[j]}$ ,  $\sigma_{t:m,\ell}^{2[j]}$  via eq. (18);
- 5: Compute extrinsic means  $\bar{\theta}_{m,k}^{[j]}$ ,  $\bar{t}_{m,\ell}^{[j]}$  via eq. (20);
- 6: Compute extrinsic variances  $\bar{v}_{\theta:m,k}^{[j]}$ ,  $\bar{v}_{t:m,\ell}^{[j]}$  via eq. (21);
- 7: Denoise the beliefs  $\tilde{\theta}_{m,k}^{[j]}$ ,  $\tilde{t}_{m,\ell}^{[j]}$  via eq. (22a);
- 8: Denoise the error variances  $\psi_{\theta:m,k}^{[j]}$ ,  $\psi_{t:m,\ell}^{[j]}$  via eq. (22b);
- 9: Update the soft-replicas with damping;
- 10: Update the effective rotation channel matrix  $\mathbf{H}_\theta$  via eq. (15);
- 11: **end for**
- 12: Obtain final consensus estimates  $\tilde{\theta}_k$ ,  $\tilde{t}_\ell$  via eq. (24);
- 13: Obtain interference-cancelled system via eq. (25);
- 14: **for**  $j = 1$  to  $j_{\max}$  **do**
- 15: Compute soft-IC symbols  $\tilde{z}_{\theta:m,k}^{[j]}$  via eq. (26a);
- 16: Compute conditional variances  $\sigma_{\theta:m,k}^{2[j]}$  via eq. (26b);
- 17: Compute extrinsic means  $\bar{\theta}_{m,k}^{[j]}$  via eq. (20a);
- 18: Compute extrinsic variances  $\bar{v}_{\theta:m,k}^{[j]}$  via eq. (21a);
- 19: Denoise the beliefs  $\tilde{\theta}_{m,k}^{[j]}$  via eq. (22a);
- 20: Denoise the error variances  $\psi_{\theta:m,k}^{[j]}$  via eq. (22b);
- 21: Update the soft-replicas with damping;
- 22: Update the effective rotation channel matrix  $\mathbf{H}_\theta$  via eq. (15);
- 23: **end for**
- 24: Obtain refined consensus estimates  $\tilde{\theta}_k$  via eq. (24a);

Such an effect can be intuitively explained by the fact that a small change in the rotation angles leads to a small change in the sensor positions, while a small change in the translation vector leads to a large change in the sensor positions, as visualized in Figure 1.

In light of the above, to counter the problem of the aforementioned error behavior of the rotation angle parameters  $\theta$ , we propose an interference cancellation-based approach to remove the components corresponding to the translation of the rigid body, and perform the GaBP again only on the rotation angle parameters. By using the estimated consensus translation vector  $\tilde{\mathbf{t}} \triangleq [\tilde{t}_1, \tilde{t}_2, \tilde{t}_3]^\top \in \mathbb{R}^{3 \times 1}$  obtained at the end of the GaBP via equation (24b), the interference-cancelled system is given by

$$\mathbf{z}'_n \triangleq \mathbf{z}_n - \mathbf{H}_t \tilde{\mathbf{t}} = \mathbf{H}_\theta \theta + \xi_n \in \mathbb{R}^{M \times 1}. \quad (25)$$

Finally, the GaBP procedure to estimate the rotation angle parameters  $\theta$  is similar to the previous steps, except for the factor node equations, which yields

$$\tilde{z}'_{\theta:m,k}^{[j]} = z'_m - \sum_{i \neq k} h_{\theta:m,i} \hat{\theta}_{m,i}^{[j]} \in \mathbb{R}, \quad (26a)$$

$$\sigma_{\theta:m,k}^{2[j]} = \sum_{i \neq k} |h_{\theta:m,i}|^2 \psi_{\theta:m,i}^{[j]} + N_0 \in \mathbb{R}. \quad (26b)$$

The second loop to refine the rotation estimates is concatenated with the bivariate GaBP to describe the complete estimation process of the rigid body transformation parameters  $\theta$  and  $t$ , as summarized by Algorithm 1.

**IV. Performance Evaluation**

To provide a comprehensive performance evaluation of the proposed GaBP-based RBL algorithm, we compare it against the SotA method based on method described in [50], which also uses GaBP for the estimation of the rigid body transformation parameters, but does not use the proposed quadratic approximation of the rotation matrix, and instead relies on the small-angle approximation. The simulation parameters are illustrated in Figure 2, where the rigid body is composed of  $N$  landmark points, whose positions are known in the local coordinate system of the rigid body, and  $M$  anchors with known absolute positions in the global coordinate system. The conformation matrix of the target rigid body is given by

$$\mathbf{C} = \begin{bmatrix} -0.5 & 0.5 & 0.5 & -0.5 & -0.5 & 0.5 & -0.5 & 0.5 \\ -0.5 & -0.5 & 0.5 & 0.5 & -0.5 & -0.5 & 0.5 & 0.5 \\ -0.5 & -0.5 & -0.5 & -0.5 & 0.5 & 0.5 & 0.5 & 0.5 \end{bmatrix} \in \mathbb{R}^{3 \times 8},$$

while the anchors conformation matrix  $\mathbf{A} \in \mathbb{R}^{3 \times 8}$  is

$$\mathbf{A} = \begin{bmatrix} -10 & 10 & 10 & -10 & -10 & 10 & -10 & 10 \\ -10 & -10 & 10 & 10 & -10 & -10 & 10 & 10 \\ -10 & -10 & -10 & -10 & 10 & 10 & 10 & 10 \end{bmatrix} \in \mathbb{R}^{3 \times 8}.$$

The rigid body parameters are generated randomly each realization, where the rotation angles  $\theta_x, \theta_y, \theta_z$  follow a zero-mean Gaussian distribution of variance  $\phi_\theta = 10\text{deg}^2$ , which is changing depending on the large or small angle scenario and the RBL translation vector elements also follow a zero-mean Gaussian distribution of variance  $\phi_t = 5\text{m}^2$ .

**A. Numerical Results**

The first set of results in Figure 5 illustrates the root mean square error (RMSE) performance of the translation vector estimate of the proposed method, compared to the SotA method of [50] that uses GaBP to estimate the rigid body parameters, which is, however, limited by the small-angle approximation used in the system model. It can be observed that, as expected, the translation vector estimate is equally well estimated by both methods, over the whole error regime. This result can be justified by the fact that the translation part of the system model is not affected by the different angle approximation used in the linearized model and thus, yields the same performance as the SotA.

The performance is evaluated by the RMSE, which is defined as

$$\text{RMSE} = \sqrt{\frac{1}{E} \sum_{i=1}^E \|\hat{\mathbf{x}}^{[i]} - \mathbf{x}\|_2^2}, \quad (27)$$

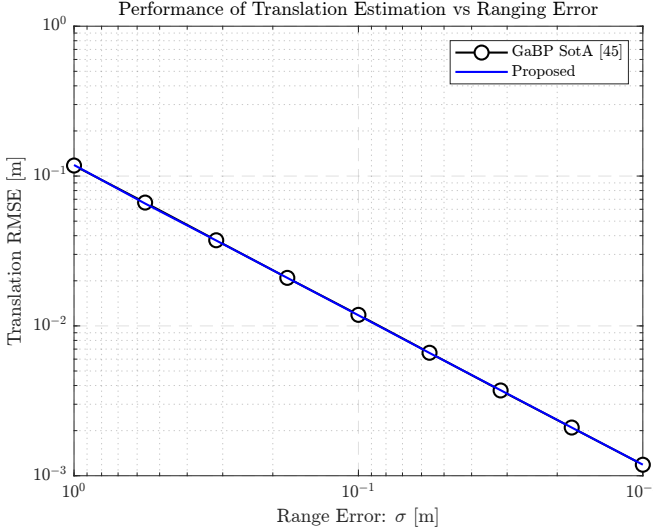


**Figure 5.** RMSE of the translation estimate of the proposed method and the SotA, over the range error  $\sigma$ .

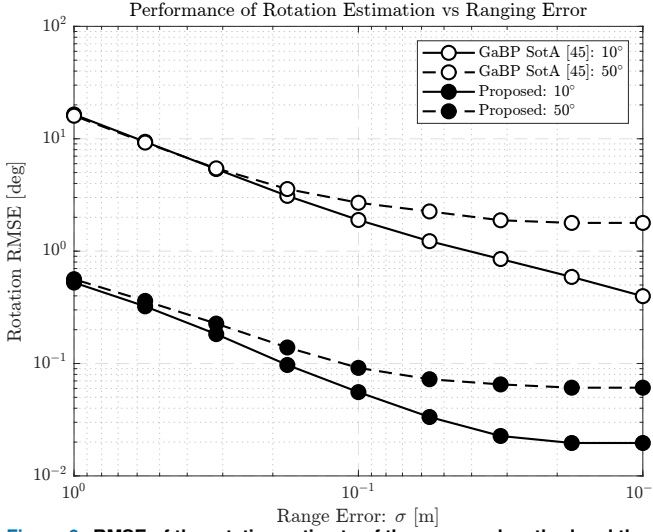


**Figure 6.** RMSE of the rotation estimate of the proposed method and the SotA, over the range error  $\sigma$ .

where  $\hat{\mathbf{x}}^{[i]}$  is the rigid body parameter vector (angle or translation) estimated during the  $i$ -th Monte-Carlo simulation,  $\mathbf{x}$  is the true RBL parameter vector, and  $E = 10^4$  is the total number of independent Monte-Carlo experiments used for the analysis, and is evaluated for different noise standard deviations  $\sigma$ . Additionally, for the GaBP algorithms, the damping factor is set to  $\rho = 0.5$ , and the maximum number of iterations is set to  $j_{\max} = 30$ , which has empirically shown sufficient convergence.

Next, in Figure 6, the RMSE performance of the rotation angle estimate is illustrated, where again, the proposed method is compared to the SotA method of [50], for different levels of the angle deviation  $\phi_\theta$ . It can be observed that the general performance of the proposed method is far superior to the SotA, especially for larger angle deviations. While the performance of the SotA degrades rapidly for larger angle deviations, the proposed method is robust to such changes, with an overall improved performance of more than one decade, over the whole noise regime.

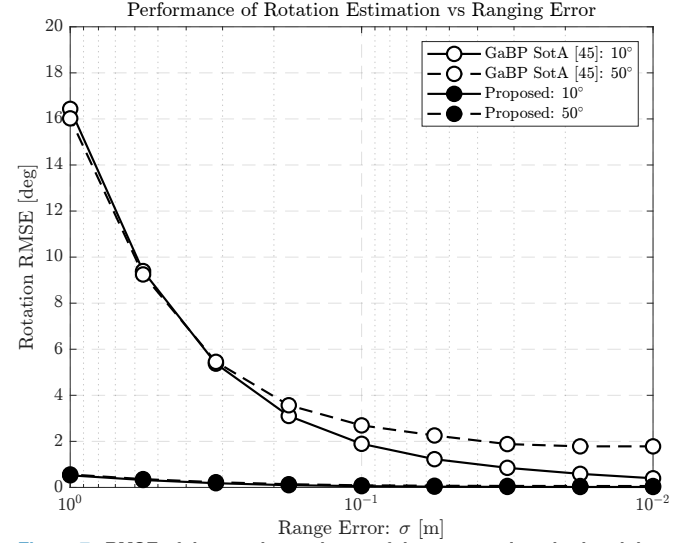


**Figure 7.** RMSE of the rotation estimate of the proposed method and the SotA, over the range error  $\sigma$ .

Finally, since the gain in terms of robustness is not clearly visible in the logarithmic scale of Figure 6, in Figure 7 the results are presented again in a linear scale. As can be observed, the proposed method maintains a low RMSE even for large angle deviations, over the whole noise regime, while the SotA method fails to provide acceptable estimates for larger angle deviations and high measurement noise.

### B. Complexity Analysis

In addition to the performance analysis, for the sake of completeness, the computational complexity of the proposed methods are compared to the SotA method of [50], given in big- $O$  notation. While the proposed method clearly outperforms the SotA methods in terms of performance, its complexity in big- $O$  notation is identical, with  $O(NMK^2)$  for both GaBP algorithms, where  $N$  is the number of landmark points,  $M$  is the number of anchors, and  $K$  is the dimension of space. The complexity compared to the SotA can be well justified, since the only difference is the iterative update of the effective channel matrix  $\mathbf{H}_\theta$  in equation (15), which does not change the overall complexity order. Finally, in terms of convergence behavior, the convergence of the rotation matrix estimate of the proposed method converges in a similar manner as the SotA, but to a lower RMSE, with both methods converging in less than 5 iterations for different noise levels  $\sigma$  and thus, a dedicated convergence figure is omitted for brevity.

### V. Conclusion

We proposed a novel RBL algorithm, capable of estimating the rigid body transformation parameters, *i.e.*, translation and rotation, with high accuracy for both small and large angle deviations, based on range measurements that utilizes a novel quadratic approximation of the rotation matrix and a double GaBP-based estimation algorithm. First, the conventional rigid body system model is linearized by using a novel quadratic approximation of the rotation matrix, which is valid for both small and large angle deviations.

$$\mathbf{Q}^{[i]} = \begin{bmatrix} \gamma^2 - \gamma\delta(\theta_y^{[i-1]}\theta_y^{[i]} + \theta_z^{[i-1]}\theta_z^{[i]}) & -\gamma\beta\theta_z^{[i]} - \gamma\alpha\theta_z^{[i-1]}\theta_z^{[i]} & \beta\theta_y^{[i]} + \alpha\theta_y^{[i-1]}\theta_y^{[i]} \\ \gamma\beta\theta_z^{[i]} + \gamma\alpha\theta_z^{[i-1]}\theta_z^{[i]} & \gamma^2 - \gamma\delta(\theta_x^{[i-1]}\theta_x^{[i]} + \theta_z^{[i-1]}\theta_z^{[i]}) & -\gamma\beta\theta_x^{[i]} - \gamma\alpha\theta_x^{[i-1]}\theta_x^{[i]} \\ -\beta\theta_y^{[i]} - \alpha\theta_y^{[i-1]}\theta_y^{[i]} & \gamma\beta\theta_x^{[i]} + \gamma\alpha\theta_x^{[i-1]}\theta_x^{[i]} & \gamma^2 - \gamma\delta(\theta_x^{[i-1]}\theta_x^{[i]} + \theta_y^{[i-1]}\theta_y^{[i]}) \end{bmatrix}, \quad (30)$$

Subsequently, a double GaBP-based estimation algorithm is proposed, employing the novel linearized system model to jointly estimate the rigid body transformation parameters. Simulation results illustrate the good performance of the proposed technique in terms of RMSE as a function of the measurement error, outperforming the SotA in all error regimes for the rotation estimate, with great accuracy for large angle derivations, while preserving the same computational complexity and convergence behavior, as well as the same performance for the translation estimation.

## Appendix A

### Linear Model Derivation

In order to prove that equation (13) is indeed equivalent to the vectorized version of the rotation matrix  $\mathbf{Q}$  given by equation (1), the formulation can be derived, starting from equation (1), applying the corresponding approximation.

Next, all the pairs of sine and cosine functions are approximated by the proposed quadratic approximation given by equation (13), which lead to the following approximations, written as

$$\cos(\theta_z) \sin(\theta_y) \approx \gamma\beta\theta_y^{[i]} + \gamma\alpha\theta_y^{[i-1]}\theta_y^{[i]}, \quad (30a)$$

$$\cos(\theta_x) \sin(\theta_z) \approx \gamma\beta\theta_z^{[i]} + \gamma\alpha\theta_z^{[i-1]}\theta_z^{[i]}, \quad (30b)$$

$$\cos(\theta_z) \sin(\theta_x) \approx \gamma\beta\theta_x^{[i]} + \gamma\alpha\theta_x^{[i-1]}\theta_x^{[i]}, \quad (30c)$$

$$\cos(\theta_x) \sin(\theta_y) \approx \gamma\beta\theta_y^{[i]} + \gamma\alpha\theta_y^{[i-1]}\theta_y^{[i]}, \quad (30d)$$

$$\cos(\theta_y) \sin(\theta_x) \approx \gamma\beta\theta_x^{[i]} + \gamma\alpha\theta_x^{[i-1]}\theta_x^{[i]}, \quad (30e)$$

$$\cos(\theta_x) \cos(\theta_z) \approx \gamma^2 - \gamma\delta(\theta_x^{[i-1]}\theta_x^{[i]} + \theta_z^{[i-1]}\theta_z^{[i]}), \quad (30f)$$

$$\cos(\theta_x) \cos(\theta_y) \approx \gamma^2 - \gamma\delta(\theta_x^{[i-1]}\theta_x^{[i]} + \theta_y^{[i-1]}\theta_y^{[i]}). \quad (30g)$$

Next, with the approximation terms in hand, all the terms are substituted into the original rotation matrix  $\mathbf{Q}$ , as defined in equation (1). The result of said substitution is described in equation (30) and can then be vectorized to yield the final result given by equation (13), described in compact matrix form, whereas the full vectorized form is given as

$$\begin{aligned} \text{vec}(\mathbf{Q}^{[i]}) &= \gamma + (\beta\mathbf{L} + \alpha\mathbf{L}\boldsymbol{\Theta} - \delta\mathbf{D}\boldsymbol{\Theta})\boldsymbol{\theta}^{[i]} \\ &= \begin{bmatrix} \gamma^2 - \gamma\delta(\theta_y^{[i-1]}\theta_y^{[i]} + \theta_z^{[i-1]}\theta_z^{[i]}) \\ \gamma\beta\theta_z^{[i]} + \gamma\alpha\theta_z^{[i-1]}\theta_z^{[i]} \\ -\beta\theta_y^{[i]} - \alpha\theta_y^{[i-1]}\theta_y^{[i]} \\ -\gamma\beta\theta_z^{[i]} - \gamma\alpha\theta_z^{[i-1]}\theta_z^{[i]} \\ \gamma\beta\theta_x^{[i]} + \gamma\alpha\theta_x^{[i-1]}\theta_x^{[i]} \\ \beta\theta_y^{[i]} + \alpha\theta_y^{[i-1]}\theta_y^{[i]} \\ -\gamma\beta\theta_x^{[i]} - \gamma\alpha\theta_x^{[i-1]}\theta_x^{[i]} \\ \gamma^2 - \gamma\delta(\theta_x^{[i-1]}\theta_x^{[i]} + \theta_y^{[i-1]}\theta_y^{[i]}) \end{bmatrix}. \end{aligned} \quad (31)$$

## References

- [1] H. Kong, C. Huang, J. Yu, and X. Shen, "A survey of mmWave radar-based sensing in autonomous vehicles, smart homes and industry," *IEEE Communications Surveys & Tutorials*, vol. 27, no. 1, pp. 463–508, 2025.
- [2] ITU-R, International Telecommunication Union - Radiocommunication Sector, "M.2160-0: Framework and overall objectives of the future development of IMT for 2030 and beyond," Nov. 2023.
- [3] J. A. Zhang, F. Liu, C. Masouros, R. W. Heath, Z. Feng, L. Zheng, and A. Petropulu, "An overview of signal processing techniques for joint communication and radar sensing," *IEEE Journal of Selected Topics in Signal Processing*, vol. 15, no. 6, pp. 1295–1315, 2021.
- [4] K. R. R. Ranasinghe, H. S. Rou, G. T. F. de Abreu, T. Takahashi, and K. Ito, "Joint channel, data and radar parameter estimation for AFDM systems in doubly-dispersive channels," 2024.
- [5] H. S. Rou *et al.*, "Integrated sensing and communications for 3D object imaging via bilinear inference," *IEEE Transactions on Wireless Communications*, vol. 23, no. 8, pp. 8636–8653, 2024.
- [6] A. Yassin, Y. Nasser, M. Awad, A. Al-Dubai, R. Liu, C. Yuen, R. Raulefs, and E. Aboutanios, "Recent advances in indoor localization: A survey on theoretical approaches and applications," *IEEE Communications Surveys & Tutorials*, vol. 19, no. 2, pp. 1327–1346, 2017.
- [7] A. Ghods and G. Abreu, "Complex-domain super MDS: A new framework for wireless localization with hybrid information," *IEEE Transactions on Wireless Communications*, vol. 17, no. 11, pp. 7364–7378, 2018.
- [8] F. Zafari, A. Gkelias, and K. K. Leung, "A survey of indoor localization systems and technologies," *IEEE Communications Surveys & Tutorials*, vol. 21, no. 3, pp. 2568–2599, 2019.
- [9] Q. D. Vo and P. De, "A survey of fingerprint-based outdoor localization," *IEEE Communications Surveys & Tutorials*, vol. 18, no. 1, pp. 491–506, 2016.
- [10] N. Führling, H. S. Rou, G. T. F. de Abreu, D. González G., and O. Gonsa, "Robust received signal strength indicator (RSSI)-based multitarget localization via gaussian process regression," *IEEE Journal of Indoor and Seamless Positioning and Navigation*, vol. 1, pp. 104–114, 2023.
- [11] M. A. G. Al-Sadoon, R. Asif, Y. I. A. Al-Yasir, R. A. Abd-Alhameed, and P. S. Excell, "AOA localization for vehicle-tracking systems using a dual-band sensor array," *IEEE Transactions on Antennas and Propagation*, vol. 68, no. 8, pp. 6330–6345, 2020.
- [12] G. Zeng, B. Mu, J. Chen, Z. Shi, and J. Wu, "Global and asymptotically efficient localization from range measurements," *IEEE Transactions on Signal Processing*, vol. 70, pp. 5041–5057, 2022.
- [13] D. Macagnano and G. T. F. de Abreu, "Algebraic approach for robust localization with heterogeneous information," *IEEE Transactions on Wireless Communications*, vol. 12, no. 10, pp. 5334–5345, 2013.
- [14] K. Eckenhoff, Y. Yang, P. Geneva, and G. Huang, "Tightly-coupled visual-inertial localization and 3-D rigid-body target tracking," *IEEE Robotics and Automation Letters*, vol. 4, no. 2, pp. 1541–1548, 2019.
- [15] B. Gebregziabher, "Multi object tracking for predictive collision avoidance," 2023.
- [16] Y. Huang, J. Du, Z. Yang, Z. Zhou, L. Zhang, and H. Chen, "A survey on trajectory-prediction methods for autonomous driving," *IEEE Transactions on Intelligent Vehicles*, vol. 7, no. 3, pp. 652–674, 2022.
- [17] T.-L. Yang, A.-X. Liu, Q. Jin, Y.-F. Luo, H.-P. Shen, and L.-B. Hang, "Position and orientation characteristic equation for topological design of robot mechanisms," *Journal of Mechanical Design*, vol. 131, no. 2, p. 021001, 2008.
- [18] W. Whittaker and L. Nastro, "Utilization of position and orientation data for preplanning and real time autonomous vehicle navigation," in *IEEE/ION Position, Location, and Navigation Symposium*, 2006.

[19] D. W. Eggert, A. Lorusso, and R. B. Fisher, "Estimating 3-D rigid body transformations: A comparison of four major algorithms," *Machine Vision and Applications*, vol. 9, no. 5, pp. 272–290, 1997.

[20] J. Diebel, "Representing attitude: Euler angles, unit quaternions, and rotation vectors," *Matrix*, vol. 58, pp. 1–35, 2006.

[21] S. P. Chepuri, A. Simonetto, G. Leus, and A.-J. van der Veen, "Tracking position and orientation of a mobile rigid body," in *2013 5th IEEE International Workshop on Computational Advances in Multi-Sensor Adaptive Processing (CAMSAP)*, 2013, pp. 37–40.

[22] S. Chen and K. C. Ho, "Accurate localization of a rigid body using multiple sensors and landmarks," *IEEE Transactions on Signal Processing*, vol. 63, no. 24, pp. 6459–6472, 2015.

[23] S. Brás, M. Izadi, C. Silvestre, A. Sanyal, and P. Oliveira, "Nonlinear observer for 3D rigid body motion estimation using doppler measurements," *IEEE Transactions on Automatic Control*, vol. 61, no. 11, pp. 3580–3585, 2016.

[24] Y. Wang, G. Wang, S. Chen, K. C. Ho, and L. Huang, "An investigation and solution of angle based rigid body localization," *IEEE Transactions on Signal Processing*, vol. 68, pp. 5457–5472, 2020.

[25] L. Zha, D. Chen, and G. Yang, "3D moving rigid body localization in the presence of anchor position errors," 2021.

[26] Q. Yu, Y. Wang, Y. Shen, and X. Shi, "Cooperative multi-rigid-body localization in wireless sensor networks using range and doppler measurements," *IEEE Internet of Things Journal*, 2023.

[27] N. Führling, H. S. Rou, G. T. F. de Abreu, D. González G., G. Seco-Granados, and O. Gonsa, "Rigid body localization and tracking for 6G V2X: Algorithms, applications, and road to adoption," 2025. [Online]. Available: <https://arxiv.org/abs/2509.01208>

[28] N. Führling, G. T. F. d. Abreu, D. González G., and O. Gonsa, "Robust egoistic rigid body localization," *IEEE Transactions on Signal Processing*, vol. 73, pp. 5076–5089, 2025.

[29] W. Chaoyi, Y. Hua, T. Song, Z. Xue, R. Ma, N. Robertson, and H. Guan, "Fine-grained pose temporal memory module for video pose estimation and tracking," in *IEEE International Conference on Acoustics, Speech and Signal Processing (ICASSP)*, 2021.

[30] Y. Xiang, T. Schmidt, V. Narayanan, and D. Fox, "Posecnn: A convolutional neural network for 6D object pose estimation in cluttered scenes," 2017, arXiv:1711.00199.

[31] F. Aghili and A. Salerno, "Driftless 3-D attitude determination and positioning of mobile robots by integration of imu with two rtk gpss," *IEEE/ASME Transactions on Mechatronics*, vol. 18, no. 1, pp. 21–31, 2013.

[32] J. Zhao, "A review of wearable imu-based pose estimation and drift reduction technologies," in *Journal of Physics: Conference Series*, vol. 1087, 2018.

[33] A. Alcocer, P. Oliveira, A. Pascoal, R. Cunha, and C. Silvestre, "A dynamic estimator on  $SE(3)$  using range-only measurements," in *IEEE Conference on Decision and Control*, 2008.

[34] S. Sand, A. Dammann, and C. Mensing, *Positioning in Wireless Communications Systems*. Wiley, 2014.

[35] N. Führling, G. Abreu, D. González G., and O. Gonsa, "SMDS-based rigid body localization," 2026. [Online]. Available: <https://arxiv.org/abs/2509.01223>

[36] J. Jiang, G. Wang, and K. C. Ho, "Accurate rigid body localization via semidefinite relaxation using range measurements," *IEEE Signal Processing Letters*, vol. 25, no. 3, pp. 378–382, 2018.

[37] G. Wang and K. C. Ho, "Accurate semidefinite relaxation method for 3-D rigid body localization using aoa," in *IEEE International Conference on Acoustics, Speech and Signal Processing (ICASSP)*, 2020.

[38] Z. Ma and K. Ho, "Toa localization in the presence of random sensor position errors," in *IEEE International Conference on Acoustics, Speech and Signal Processing (ICASSP)*, 2011.

[39] K. Ho and W. Xu, "An accurate algebraic solution for moving source location using tdoa and fdoa measurements," *IEEE Transactions on Signal Processing*, vol. 52, no. 9, pp. 2453–2463, 2004.

[40] T. Vaskevicius and N. Zhivotovskiy, "Suboptimality of constrained least squares and improvements via non-linear predictors," *Bernoulli*, 2023.

[41] O. Y. Feng, R. Venkataramanan, C. Rush, and R. J. Samworth, *A Unifying Tutorial on Approximate Message Passing*. Now Publishers, 2022.

[42] X. Zhu, Y. Ma, X. Li, and T. Li, "Alternating subspace approximate message passing," 2024, arXiv:2407.07436.

[43] J. T. Parker, P. Schniter, and V. Cevher, "Bilinear generalized approximate message passing—part i: Derivation," *IEEE Transactions on Signal Processing*, vol. 62, no. 22, pp. 5839–5853, 2014.

[44] —, "Bilinear generalized approximate message passing—part ii: Applications," *IEEE Transactions on Signal Processing*, vol. 62, no. 22, pp. 5854–5867, 2014.

[45] H. S. Rou *et al.*, "Asymmetric bilinear inference for joint communications and environment sensing," in *Asilomar Conference on Signals, Systems, and Computers*, 2022, pp. 1111–1115.

[46] D. Jin, F. Yin, C. Fritzsche, F. Gustafsson, and A. M. Zoubir, "Bayesian cooperative localization using received signal strength with unknown path loss exponent: Message passing approaches," *IEEE Transactions on Signal Processing*, vol. 68, pp. 1120–1135, 2020.

[47] W. Yuan, N. Wu, B. Etzlinger, H. Wang, and J. Kuang, "Cooperative joint localization and clock synchronization based on gaussian message passing in asynchronous wireless networks," *IEEE Transactions on Vehicular Technology*, vol. 65, no. 9, pp. 7258–7273, 2016.

[48] Z. Yu, J. Li, Q. Guo, and J. Ding, "Efficient direct target localization for distributed mimo radar with expectation propagation and belief propagation," *IEEE Transactions on Signal Processing*, vol. 69, pp. 4055–4068, 2021.

[49] V. Vizitiv, H. S. Rou, N. Führling, and G. T. F. de Abreu, "Belief propagation-based rotation and translation estimation for rigid body localization," in *Proc. IEEE Wireless Communications and Networking Conf. (WCNC)*, 2025.

[50] N. Führling, V. Vizitiv, K. R. R. Ranasinghe, H. S. Rou, G. T. F. d. Abreu, D. González G., and O. Gonsa, "6D rigid body localization and velocity estimation via gaussian belief propagation," *IEEE Transactions on Signal Processing*, vol. 73, pp. 3902–3917, 2025.

[51] J. Diebel, "Representing attitude: Euler angles, unit quaternions, and rotation vectors," *Matrix*, vol. 58, no. 15–16, pp. 1–35, 2006.

[52] K. Ho and W. Xu, "An accurate algebraic solution for moving source location using tdoa and fdoa measurements," *IEEE Transactions on Signal Processing*, vol. 52, no. 9, pp. 2453–2463, 2004.

[53] Z. Ma and K. Ho, "Toa localization in the presence of random sensor position errors," in *IEEE International Conference on Acoustics, Speech and Signal Processing (ICASSP)*, 2011.

[54] D. W. Eggert, A. Lorusso, and R. B. Fisher, "Estimating 3-D rigid body transformations: A comparison of four major algorithms," *Machine Vision and Applications*, vol. 9, no. 5, pp. 272–290, 1997.

[55] L. Zha, D. Chen, and G. Yang, "3D moving rigid body localization in the presence of anchor position errors," 2021, preprint.